This work showed that the eddy viscosity component is still dominant even when stratification is present. Particularly, the turbulent mean component dominates the overall eddy viscosity component under stratified conditions. In contrast, under unstratified conditions, the contribution of the tidal straining component to the total eddy viscosity component outweighs that of other components. The authors presented a lot of figures in their work to show the results and findings (i.e., 17 figures in total). However, the authors are encouraged to more selective with the figures. The authors did a good job in presenting interesting experiments and results to the scientific community. However, as there are a few things requiring improvement in the manuscript at this point, it is suggested that the article should go through minor revisions and English editing before accepting and publishing. Specific review comments are provided to the authors as follows.

Response: We would like to thank you for your careful reading, helpful comments, and constructive suggestions, which have significantly improved the presentation of our manuscript. We appreciate all your professional comments and have revised our manuscript accordingly. The original 17 figures have been consolidated into 13, and Table 2 has been transformed into a bar chart, bringing the total number of figures to 14 in the revised manuscript (figures appended at the end). Additionally, we have made further revisions and refined the English based on the reviewer's suggestions.

Lines 059 – 059: It should be "gravitational circulation" instead of "gravity circulation".

Response: The "gravity circulation" has been changed into "gravitational circulation" (line 59).

Lines 061 – 062: It is understood that the authors already provided brief comparison in lines 086 – 090. However, the authors are encouraged to provide a brief introduction and definition of ERV and LRV when they first appeared in the paper. For example, one of the authors' previous works published on the Frontiers in Marine Science (Deng et al., 2022; https://doi.org/10.3389/fmars.2022.901490) mentioned that "Eulerian residual velocity (ERV) is the average of the velocities during one or several tidal periods at a fixed location (Abbott, 1960). Lagrangian residual velocity (LRV) is defined as the net displacement of a labeled water parcel over one or several tidal periods (Zimmerman, 1979)."

Response: In the revised manuscript, concise definitions of ERV (lines 61–63) and LRV (lines 103–105) have been included at their initial mentions in the paper. "*To remove the tidal signal, early researchers such as Abbott (1960) utilized a straightforward method by averaging current velocities over one or several tidal periods at a specific location to calculate the Eulerian Residual Velocity (ERV).*" "*Zimmerman (1979) defined Lagrangian residual velocity (LRV) as the net displacement of the water parcels over one or several tidal periods.*"

Lines 077 – 085: While several relevant works have been reviewed and included, the

authors are encouraged to include some most-recent studies. For example, Hewageegana et al. (2023; https://doi.org/10.3390/jmse11071333) used a numerical model (ROMS) to analyze the seasonal variation of residence time at Caloosahatchee River Estuary, Florida during a period of five years. Hewageegana et al. (2023) discovered and showed a relationship between residence time and wind direction and magnitude.

Response: The most recent studies have been induced in the revised manuscript (lines 80–90; lines 96–99; lines 108–122; lines 160–162). "*Wind, in conjunction with tides and density gradients, exerts a substantial influence on estuarine residual currents and stratification (Verspecht et al., 2009; Jongbloed et al., 2022). Its role in the generation of surface residual currents is underscored by the strong correlations observed between wind speeds and residual current velocities across both annual and seasonal timescales (Ren et al., 2022). Research on the Dongsha atoll revealed that the combined effects of wind and tide introduce more dynamic water exchange compared to tides alone (Chen, 2023). In the Bohai Sea area off Qinhuangdao, residual currents exhibit pronounced seasonal fluctuations, correlating notably with wind speeds at specific temporal lags (Zhang et al., 2023). Furthermore, the shift in wind-driven circulation is pivotal for mass transport within bays, with estuarine residual circulation superseding tidal pumping as the primary transport mechanism (Young et al., 2023).*"

"*Wind plays a pivotal role in modulating classical gravitational circulation, most notably reversing surface outflow during winter. In contrast, northward winds in spring enhance stratification and augment the pressure gradient-driven flow (Soto-Riquelme et al., 2023).*"

"*Lagrangian particle tracking methods play a pivotal role in studying mass transport and residence time (RT) across various coastal seas, estuaries, and bays. Specific water mass transport patterns are discerned in the Bohai Sea, revealing salient regional transport characteristics steered by LRV (Yu et al., 2023). The combined effects of residual transport velocity in the current and next seasons emerge as the predominant factor driving the RT's seasonal variation (Lin et al, 2022). Wind direction, wind speed, and density gradient-induced circulation collectively regulate RT (Hewageegana et al., 2023). The reduction of cross-shore currents results in mass convergence and increases RT (Li et al., 2022). The water exchange and RT are mainly determined by the structure of the LRV (Jiang and Feng, 2014). RT predominantly represents an accumulative measure, primarily influenced by residual transport rather than immediate responses (Jiang, 2023). Convergence zones resulting from LRV efficiently establish consistent aggregation regions of buoyant material within the estuary rather than ERV (Kukulka and Chant, 2023). To gain an in-depth understanding of mass transport, extensive prior research has been dedicated to elucidating qualitative and quantitative evaluations of the determinants impacting the LRV's*

structure and magnitude."

    "*An anticlockwise shift in summertime wind direction from 1979 to 2020 weakens cross-channel wind-driven transport and along-channel seaward flow, leading to increased stratification near the Modaomen (Hong et al. 2022).*"

Lines 177 – 178: It is recommended to write it as either "tidal periodic oscillation currents" or "periodic oscillation tidal currents". In other words, use one "tidal" instead of two.

Response: The "tidal periodic oscillation tidal currents" has changed into "tidal periodic oscillation currents" (lines 210–211).

Lines 195 – 206: The authors indicated the model setup in detail in this section. However, the authors are encouraged to indicate more about how the resolution in space and time were determined. For example, did the model setup follow some previous studies? (If yes, please include the reference.) Or did the authors perform a sensitivity analysis on computational grid resolution for this work?

Response: Yes, the resolutions in space and time for model setup are based on previous studies. The references are added to the revised manuscript (lines 247–249). "*On the other hand, the fine grid, consisting of 45,368 nodes and 87,179 triangular elements, is configured based on the settings from previous studies. (e.g., Lai et al., 2018; Geyer et al., 2020; Xu et al., 2021).*" For instance, Geyer et al. (2020) employed an average grid spacing of 100 meters in the cross-estuary direction and 165 meters in the along-estuary direction while investigating exchange flow mechanisms in Delaware Bay. Xu et al. (2021) used resolutions ranging from 100 in the inlets to 3000 meters along the coastal ocean when exploring the nonlinearity of residual currents in the Pearl River estuary (PRE). Lai et al. (2018) utilized resolutions varying from 0.1 to 10 kilometers across the entire domain: 0.1–0.3 kilometers inside the Pearl River Estuary, 0.3–0.5 kilometers at the estuary mouth, 1.0–2.0 kilometers in Guangdong coastal waters, and 10 kilometers near the open boundary to examine the impact of tides and winds on Eulerian residual velocity. Considering computational efficiency and drawing on insights from prior research in real estuaries and bays, the paper adopts specific grid resolutions. Specifically, fine grids with a resolution of 0.1 kilometers are utilized within the PRE, the primary focus area, as well as 0.1 to 1.0 kilometers off the Guangdong coast and 2.0 kilometers near the open boundary.

    The temporal resolution must adhere to the Courant-Friedrichs-Lewy (CFL) condition when spatial resolutions are specified. In theory, considering the spatial resolution and water depth in the PRE, the CFL value should ideally be less than 4 seconds. However, in practice, an external time step of 0.5 seconds is chosen to maintain model stability, especially when dealing with triangular grids and intricate topography and coastlines. Additionally, a split number of 10 is applied under these conditions when a split-mode time-stepping method is used.

Lines 210 – 215: The authors are encouraged to indicate both references and links. The authors are also encouraged to indicate the time interval (i.e., resolution in time) of the CCMP data. Additionally, the authors are encouraged to indicate the full name of "CCMP" as it appeared in the document for the first time.

Response: In the revised manuscript, we have provided the references and links for these datasets, specified the time interval for the CCMP data, and included the full name of CCMP (lines 256–274). "*The model incorporates eight major tidal constituents, namely M_2, N_2, S_2, K_2, K_1, O_1, P_1, and Q_1, as tidal driving forces at the open boundary. These constituents are obtained from the Oregon State University Tidal Prediction Software (OTPS/TPXO; https://www.tpxo.net/otps; Egbert and Svetlana, 2002). To initialize the model, salinity climatological data from the 1° World Ocean Atlas 2009 (WOA2009) dataset is utilized (https://accession.nodc.noaa.gov/0094866; Levitus, 2013). The wind data used in this study are obtained from the monthly averaged Cross-Calibrated Multi-Platform (CCMP) dataset, which has spatial resolutions of 0.25×0.25 degrees (http://www.remss.com/measurements/ccmp; Mears et al., 2022). The Pearl River Estuary (PRE) experiences seasonal reversing monsoonal winds, as documented by Pan et al. (2014) and Pan and Gu (2016). The monthly-averaged CCMP wind data indicate prevalent southwesterly winds during the summer season. Our investigation specifically focuses on the impact of southwesterly winds on the dynamics of Lagrangian Residual Velocity (LRV). The lateral boundary incorporates monthly average river runoff data from eight river inlets, which are provided by the Water Conservancy Committee of the Pearl River under the Ministry of Water Resources. The topography data off the PRE is from the ETOPO2 dataset of NOAA (https://www.ngdc.noaa.gov/mgg/global/relief/-ETOPO2/ETOPO2v2-2006/; NOAA National Geophysical Data Center, 2006), while the topography within the estuary is derived from electronic nautical chart data provided by the China Maritime Safety Administration.*"

Lines 223 – 223: The authors are encouraged to indicate the date, e.g., 1 June 2017.

Response: The specific dates have been included in the revised manuscript (line 278). "*The fine grid model, which begins on 1 June 2017*"

Lines 242 – 242: It should be "… including three cross sections (Sections B – D)".

Response: Yes, it should be "*The paper selects four sections, including three cross sections (Sections B–D)*" (lines 296–297).

Lines 245 – 249: According to the description in lines 241 – 244, should these along-estuary distributions of salinity be extracted from Section A instead of Section C? It may be clearer to move the texts in the subplots' titles "CTD" and "MODEL" to the space after "(b)" and "(c)" in the plots. In other words, the authors are encouraged to revise "(b)" as "(b) CTD" and revise "(c)" as "(c) MODEL" on the plots. Additionally, although the authors have indicated that the colormap represents salinity in the figure

caption, it may be clearer to indicate that beside the color bar as well.

Response: Along-estuary salinity distributions are sourced from CTD observation stations, with the station layout closely matching Section A. Associated captions have been updated accordingly (lines 306–307). "*(b) Along-estuary salinity profiles based on CTD depth-profiled data, closely aligned with Section A; (c) salinity outputs from the numerical model.*"

In the initial manuscript, lines 241–244 highlight that "*The examination of LRV components and the eddy viscosity subcomponent is presented solely in Section C, given the uniform conclusions derived across four sections. Moreover, the chosen cross-section, Section C, aptly depicts the differential dynamics of LRV between the shoal and the deep channel*", which has been rephrased for clarity in the updated manuscript (lines 298–302)

In the revised manuscript, the titles "CTD" and "MODEL" in Figs. 2b and c have been updated to "(b) CTD" and "(c) Model", respectively. Additionally, the caption adjacent to the color bar has been changed from "(psu)" to "Salinity (psu)".

Lines 250 – 250: It may be clearer to revise the "model-derived elevation" as "model-derived sea surface elevation".

Response: The term "model-derived elevation" has been modified to "model-derived sea surface elevation" (line 308). "*Model verification involves comparing the model-derived sea surface elevation……*"

Lines 267 – 267: It should be "good performance" instead of "well performance".

Response: The term "well performance" has been revised to "good performance" (line 326).

Lines 268 – 268: It may be clearer to represent the y-label as "Sea surface elevation" instead of "Sea level", which is also consistent with the description in line 252.

Response: The label on the y-axis in Figure 3 has been updated from "Sea level" to "Sea surface elevation."

Lines 275 – 275: It should be rewritten as "where abs is the absolute value function …".

Response: The sentence "where abs are the absolute value function" has been modified to "where abs is the absolute value function" (line 334).

Lines 294 – 299: While panels (a) to (e) in Figure 4 have been introduced in the figure caption, panels (f) to (j) are NOT introduced. Additionally, although the authors have indicated that the colormap represented uL in the figure caption, it may be clearer to indicate that beside the color bar as well. This comment also applies to Figures 5 – 17.

Response: In Fig. 4, the panels in the right columns have been detailed in the figure captions, and the associated annotations adjacent to the color bar have been updated in the revised manuscript. Analogous modifications have been implemented in other figures (Fig. 5–14) in the revised manuscript.

Lines 306 – 307: This comment is optional. The authors are encouraged to think about

how to better present the data shown in Table 2 to the readers. Would it be more appropriate and clearer if these data/numbers are presented using bar charts or something similar?

Response: Table 2 has been substituted with bar charts.
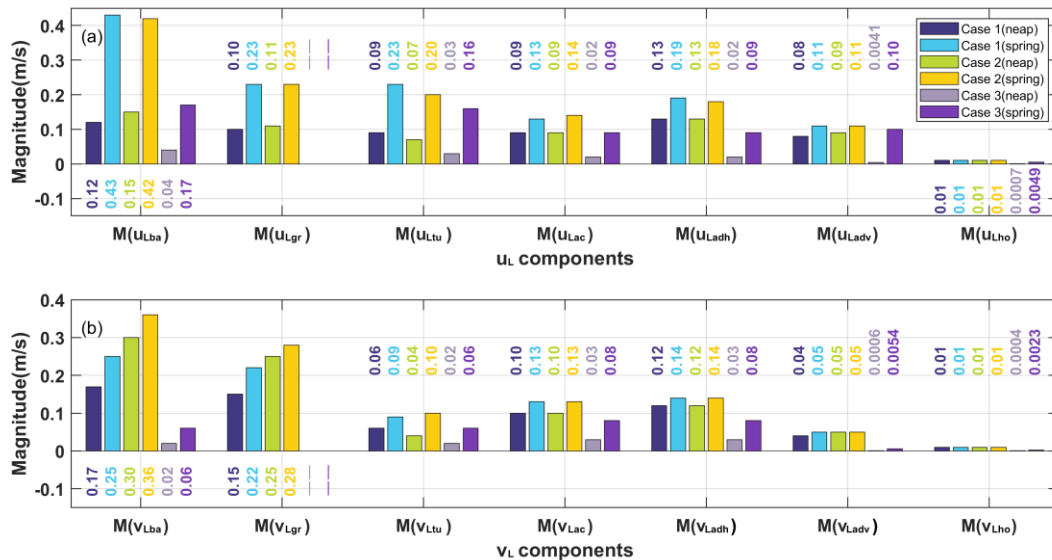
Figure 5 Bar charts for the magnitude of each component of u_L and v_L.

Lines 402 – 402: The authors are encouraged to use numbers to describe/rephrase "significant changes" or "there is no significant change" throughout the document e.g., lines 454, 489, 605, 646, 668, and 748).

Response: We have replaced the phrases "significant changes" and "there is no significant change" by quantitative values (lines 495–497; lines 531–534; lines 648–650; lines 684–687; lines 720–722; lines 746–749; lines 757–764; lines 822–823). *"with the exception of the noticeably reduced along-estuary eddy viscosity component (v_{Ltu}) by one order of magnitude in the upper layer in Case 2 during neap tides (Fig. 9g) and slightly intensified during spring tides (Fig. 9n) compared to scenarios with wind."* *"the findings indicate that the cross-estuary eddy viscosity component modulates the configuration of the cross-estuary LRV. In the upper layers, this component exhibits an enhancement of an order of magnitude under the influence of the dominant southwesterly winds, relative to conditions in the absence of wind in the PRE."* *"However, during neap tides, their magnitudes in the upper layer manifest a reduction by an order of magnitude relative to Case 1. This indicates a substantial influence of wind on these subcomponents during relatively small tides."* *"The results elucidate the substantial effect of stratification on each non-dominant component of the eddy viscosity due to the differentially sheared structure, with magnitudes an order greater than in non-stratified scenarios."* *"The results in the paper have indicated that the contribution of the horizontal diffusion component is several-fold lower, or even an*

order of magnitude less, than other components." "The findings underscore that the southwesterly wind amplifies the relative contribution ratios of the tidal straining component to the baroclinic pressure gradient component of the LRV. Specifically, these ratios are 1.5 to 3 times greater compared to scenarios without wind forcing." "This paper reveals that under stratified conditions, the tidal mean component dominates the eddy viscosity, even though the magnitudes of tidal straining and the combined component of tidal-average eddy viscosity and velocity gradient oscillation are greater than the turbulent mean component. However, these two components exhibit inverse structures of equal magnitude. As a result, their collective impact on the total eddy viscosity component is minimal or negative. Under homogeneous conditions, the tidal straining component dictates the structure of the eddy viscosity. Similarly, the cumulative effects of other components contribute negatively and minimally." "The along-estuary non-dominant components exhibit consistent magnitudes and structures, irrespective of the presence or absence of wind forcing,…..."

Lines 717 – 763: The authors are encouraged to link the finding of the resent work to some other recent studies mentioned in the INTRODUCTION. Besides, the authors are encouraged to indicate how much the tidal straining component takes precedence over other factors in line 761 using numbers or percentages.

Response: The results of the current study have been contextualized with recent research highlighted in the introduction. (lines 788–791; lines 793–795; lines 798–800; lines 835–837). *"the primary mechanisms governing the LRV in the PRE under conditions of stratification and wind are elucidated, which has been not extensively explored in prior studies (Chu et al., 2022; Deng et al., 2022)." "Notably, the decomposition methodologies rooted in Lagrangian theory adopted in this work differ from earlier studies anchored in Eulerian theory (e.g., Burchard et al., 2011; Cheng et al., 2011; Wei et al., 2021)." "While many studies have focused on ERV in the PRE (e.g., Lai et al., 2018; Xu et al., 2021; Hong et al., 2022), research on LRV in the PRE remains limited, particularly regarding the dynamic mechanisms of LRV." "Specifically, under stratified conditions, the turbulent mean component plays a dominant role in the total eddy viscosity component, which has not yet been studied in previous works (e.g., Burchard et al., 2023)."*

The magnitude of tidal straining has been quantitatively compared to other non-dominant components (lines 839–840). *"its magnitude is either several times or one order of magnitude bigger than the other components."*

Reference

Abbott, M. R.: Boundary layer effects in estuaries, J. Mar. Res., 18, 83–100, 1960.

Burchard, H., Bolding, K., Lange, X., Osadchiev, A.: Decomposition of Estuarine Circulation and Residual Stratification under Landfast Sea Ice, J. Phys. Oceanogr., 2023, 53(1), 57–80, 2023.

Burchard, H., Hetland, R. D., Schulz, E., Schuttelaars, H. M.: Drivers of residual estuarine circulation in tidally energetic estuaries: Straight and irrotational channels with parabolic cross section, J. Phys. Oceanogr., 41(3), 548–570, https://doi.org/10.1175/2010JPO4453.1, 2011.

Chen, S. M.: Water Exchange Due to Wind and Waves in a Monsoon Prevailing Tropical Atoll, J. Mar. Sci. Eng., 11(1), 109, 2023.

Cheng, P., Valle-Levinson, A., de Swart, H. E.: A numerical study of residual circulation induced by asymmetric tidal mixing in tidally dominated estuaries, J. Geophys. Res.: Oceans, 116(C1), https://doi.org/10.1029/2010JC006137, 2011.

Chu, N. Y., Liu, G. L., Xu, J., Yao, P., Du, Y., Liu, Z. Q., Cai, Z. Y.: Hydrodynamical transport structure and lagrangian connectivity of circulations in the Pearl River Estuary, Front. Mar. Sci., 9, 996551, https://doi.org/10.3389/fmars.2022.996551, 2022.

Deng, F. J., Jiang, W. S., Zong, X. L., Chen, Z. Y.: Quantifying the Contribution of Each Driving Force to the Lagrangian Residual Velocity in Xiangshan Bay, Front. Mar. Sci., 9, 901490, https://doi.org/10.3389/fmars.2022.901490, 2022.

Egbert, G. D., Erofeeva, S. Y.: Efficient inverse modeling of barotropic ocean tides, J. Atmos. Ocean. Technol., 19(2), 183–204, 2002.

Geyer, W. R., Ralston, D. K., Chen, J. L.: Mechanisms of exchange flow in an estuary with a narrow, deep channel and wide, shallow shoals, J. Geophys. Res.: Oceans, 125, e2020JC016092, https://doi.org/10.1029/2020-JC016092, 2020.

Hewageegana, V. H., Olabarrieta, M., Gonzalez-Ondina, J. M.: Main Physical Processes Affecting the Residence Times of a Micro-Tidal Estuary, J. Mar. Sci. Eng., 11(7): 1333, 2023.

Hong, B., Xue, H. L., Zhu, L. S., Xu, H. Z.: Climatic Change of Summer Wind Direction and Its Impact on Hydrodynamic Circulation in the Pearl River Estuary, J. Mar. Sci. Eng., 10, 10070842, https://doi.org/10.3390/jmse10070842, 2022.

Jiang, M. S.: Modeling Water Residence Time and Connectivity in the Northern Indian River Lagoon, Estuaries Coasts, 1-20, 2023.

Jiang, W. S., Feng, S. Z.: 3D analytical solution to the tidally induced Lagrangian residual current equations in a narrow bay, Ocean Dyn., 64, 1073–1091, https://doi.org/10.1007/s10236-014-0738-1, 2014.

Jongbloed, H., Schuttelaars, H. M., Dijkstra, Y. M., Donkers, P. B., Hoitink, A. J.: Influence of wind on subtidal salt intrusion and stratification in well-mixed and partially stratified estuaries, J. Phys. Oceanogr., 52(12), 3139–3158, https://doi.org/10.1175/JPO-D-21-0291.1, 2022.

Kukulka, T., Chant, R. J.: Surface convergence zones due to Lagrangian residual flow in tidally driven estuaries, J. Phys. Oceanogr., 53(2), 423-431, 2023.

Lai, W. F., Pan, J. Y., Devlin, A. T.: Impact of tides and winds on estuarine circulation in the Pearl River Estuary, Cont. Shelf Res., 168, 68–82, https://doi.org/10.1016/j.csr.2018.09.004, 2018.

Levitus, S., Antonov, J. I., Baranova, O. K., Boyer, T. P., Coleman, C. L., Garcia, H. E., Grodsky, A. I., Johnson, D. R., Locarnini, R. A., Mishonov, A. V., Reagan, J. R., Sazama, C. L., Seidov, D., Smolyar, I., Yarosh, E. S., Zweng, M. M.: The world ocean database. Data Science Journal, 12, WDS229-WDS234, 2013.

Li, S. Z., Zhang, Z. R., Zhou, M., Wang, C. N., Wu, H., Zhong, Y. S.: The role of fronts in horizontal transports of the Changjiang River plume in summer and the implications for phytoplankton blooms, J. Geophys. Res.: Oceans, 127(8), e2022JC018541 2022.

Lin, L., Liu, D. Y., Fu, Q. J., Guo, X. Y., Liu, G. L., Liu, H., Wang, S. L.: Seasonal variability of water residence time in the Subei Coastal Water, Yellow Sea: The joint role of tide and wind, Ocean Model., 180, 102137, https://doi.org/10.1016/j.ocemod.2022.102137, 2022.

Mears, C., Lee, T., Ricciardulli, L., Wang, X. C., Wentz, F.: Rss cross-calibrated multi-platform (Ccmp) 6-hourly ocean vector wind analysis on 0.25 deg grid, version 3.0, Remote Sens., Syst, 2022.

NOAA National Geophysical Data Center.: 2-minute Gridded Global Relief Data (ETOPO2) v2. NOAA National Centers for Environmental Information, https://doi.org/10.7289/V5J1012Q, 2006.

Pan, J. Y., Gu, Y. Z.: Cruise observation and numerical modeling of turbulent mixing in the Pearl River estuary in summer, Cont. Shelf Res., 120, 122-138, 2016.

Pan, J. Y., Gu, Y. Z., Wang, D. X.: Observations and numerical modeling of the Pearl River plume in summer season, J. Geophys. Res.: Oceans, 119, 2480–2500, https://doi.org/10.1002/2013JC009042, 2014.

Ren, L., Yang, L. N., Pan, G. W., Zheng, G., Zhu, Q., Wang, Y. Q., Zhu, Z. C., Hartnett, M.: Characterizing Residual Current Circulation and Its Response Mechanism to Wind at a Seasonal Scale Based on High-Frequency Radar Data, Remote Sens., 14, 14184510, https://doi.org/10.3390/rs14184510, 2022.

Soto-Riquelme, C., Pinilla, E., Ross, L.: Wind influence on residual circulation in Patagonian channels and fjords, Cont. Shelf Res., 254, 104905, 2023.

Verspecht, F., Rippeth, T. P., Howarth, M. J., Souza, A. J., Simpson, J. H., Burchard, H.: Processes impacting on stratification in a region of freshwater influence: Application to Liverpool Bay, J. Geophys. Res.: Oceans, 114(C11), https://doi.org/10.1029/2009JC005475, 2009.

Wei, X. Y., Schuttelaars, H. M., Williams, M. E., Brown, J. M., Thorne, P. D., Amoudry, L. O.: Unraveling interactions between asymmetric tidal turbulence, residual circulation, and salinity dynamics in short, periodically weakly stratified estuaries, J. Phys. Oceanogr., 51(5), 1395–1416, https://doi.org/10.1175/JPO-D-20-0146.1, 2021.

Xu, H. Z., Shen, J., Wang, D. X., Luo, L., Hong, B.: Nonlinearity of subtidal estuarine circulation in the Pearl River Estuary, China, Front. Mar. Sci., 8, 629403, https://doi.org/10.3389/fmars.2021.629403, 2021.

Young, J. S., Hoon, Y. K., Jongseong, R., Kyung, H. H.: Wind-induced switch of estuarine residual circulations and sediment transport in microtidal bay, Estuar. Coast. Shelf Sci., 288, 2023.

Yu, J. Z., Zhang, X. Q., Sheng, X. X., Jiang, W. S.: Mass transport pattern and mechanism in the tide-dominant Bohai Sea, Ocean Model., 182, 2023.

Zhang, D. Q., Pang, C. G., Liu, Z. L., Jiang, J. B.: Winter and summer sedimentary dynamic process observations in the sea area off Qinhuangdao in the Bohai Sea, China, Front. Earth Sci., 11, 1097033, https://doi.org/10.3389/feart.2023.1097033, 2023.

Zimmerman, J. T. F.: On the Euler-Lagrange transformation and the Stokes' drift in the presence of oscillatory and residual currents, Deep-Sea Res., 26A, 505–520, 1979.

Figures
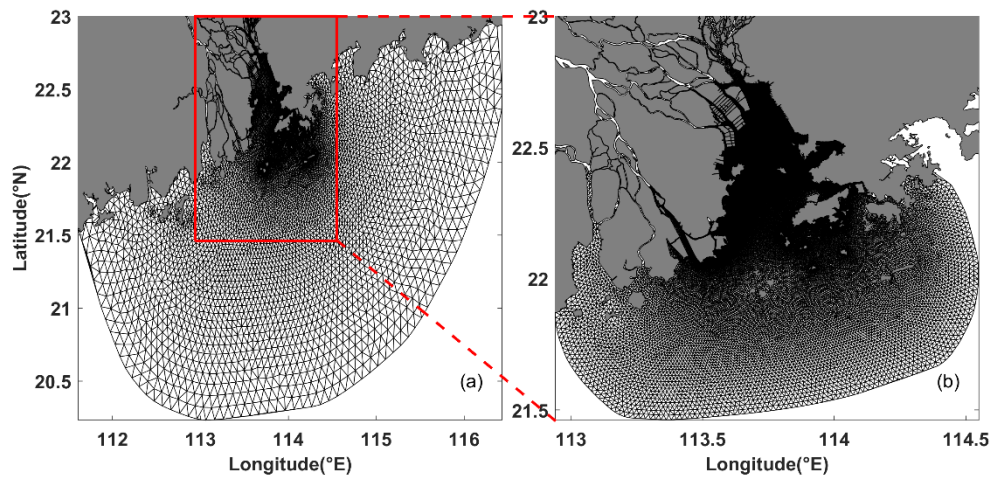
Figure 1 (a) Coarse mesh model, **(b)** fine mesh model.
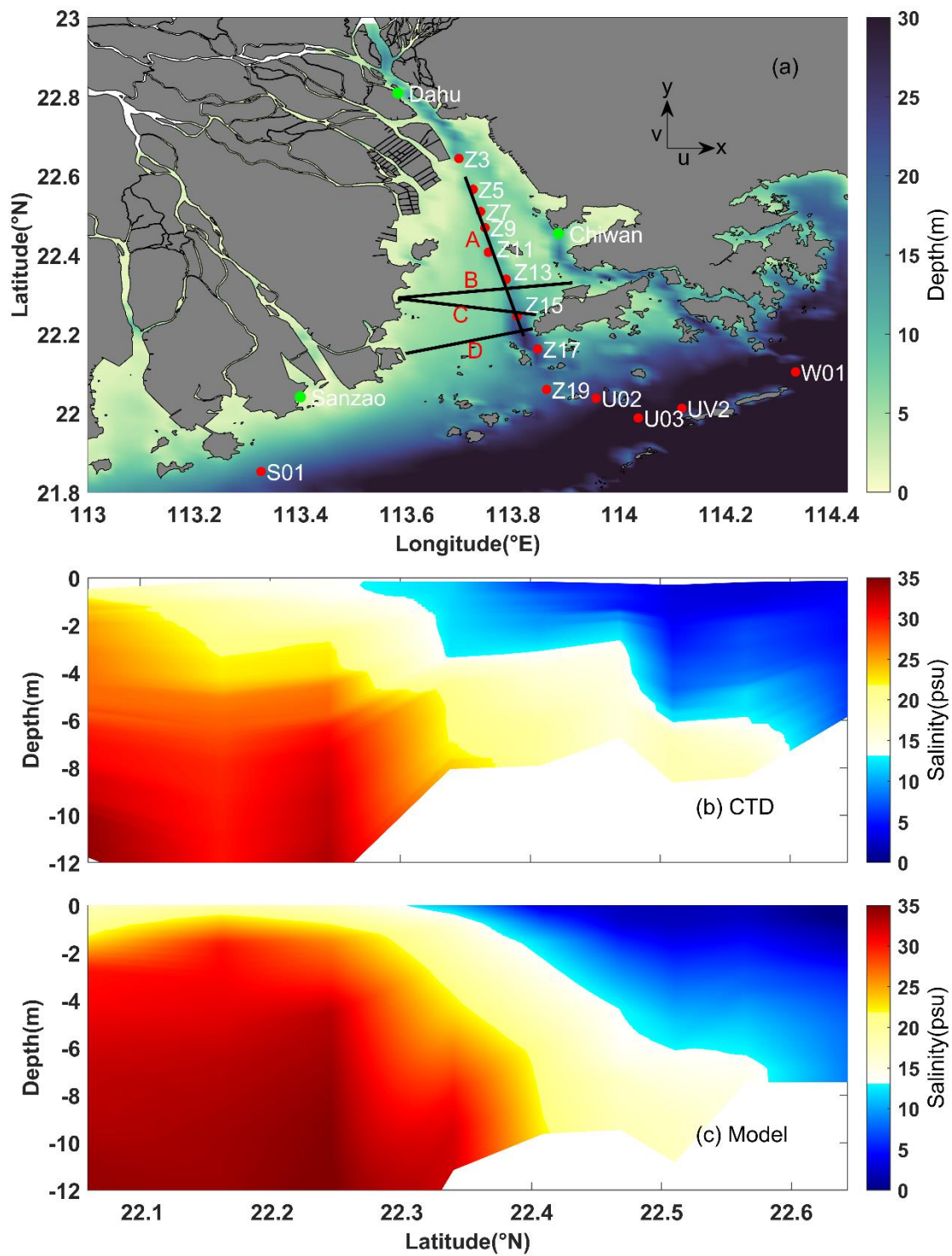
Figure 2 (a) Bathymetry of the model domain. Black lines mark sections for result analysis. Green dots indicate tide gauge stations for elevation validation, and red dots indicate CTD positions for salinity verification. **(b)** Along-estuary salinity profiles based on CTD depth-profiled data, closely aligned with Section A; **(c)** salinity outputs from the numerical model.
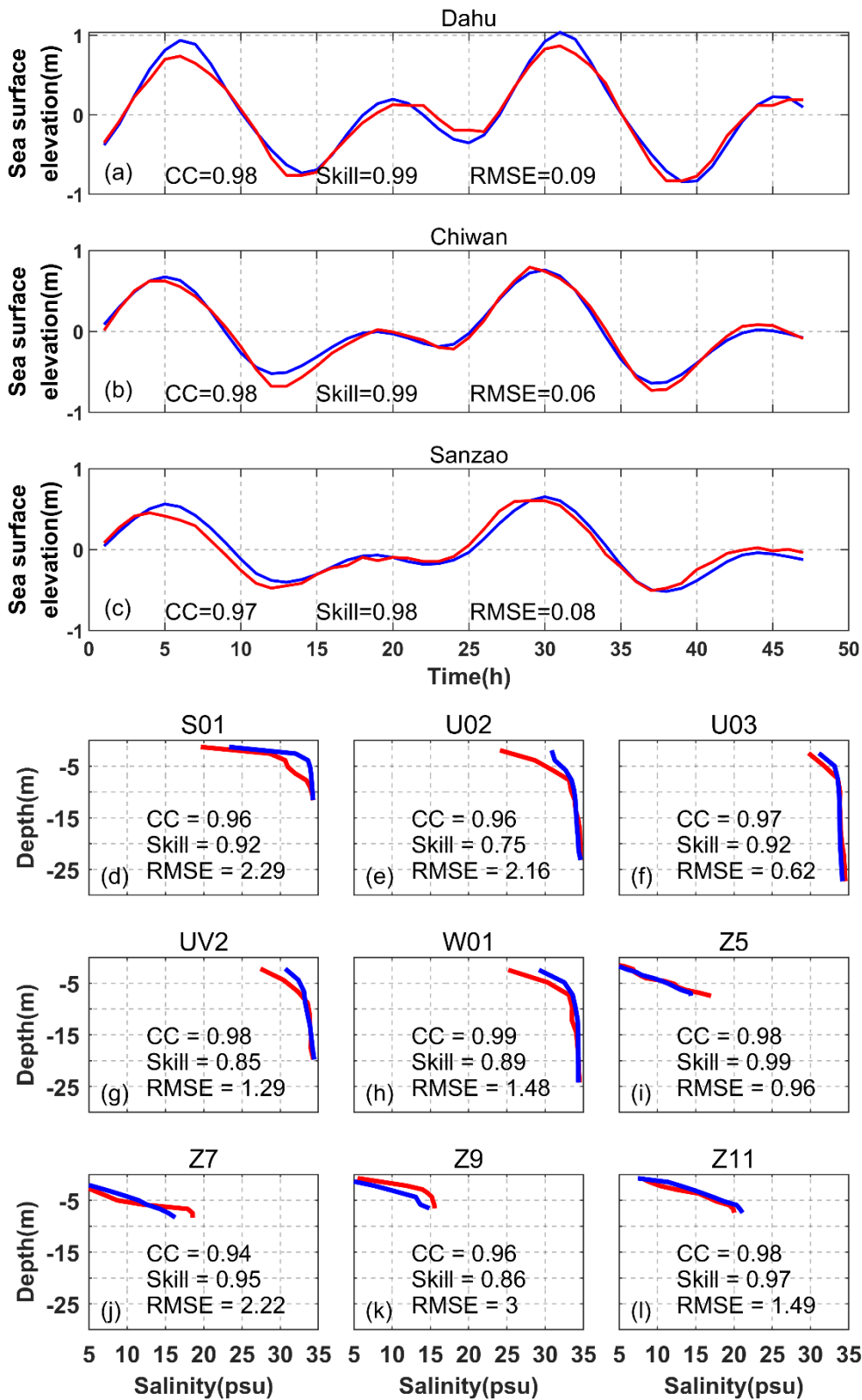
Figure 3 Comparisons between the observed (red line) and modeled (blue line) elevation and salinity. The three parameters including CC, Skill, and RMSE are calculated at each station.
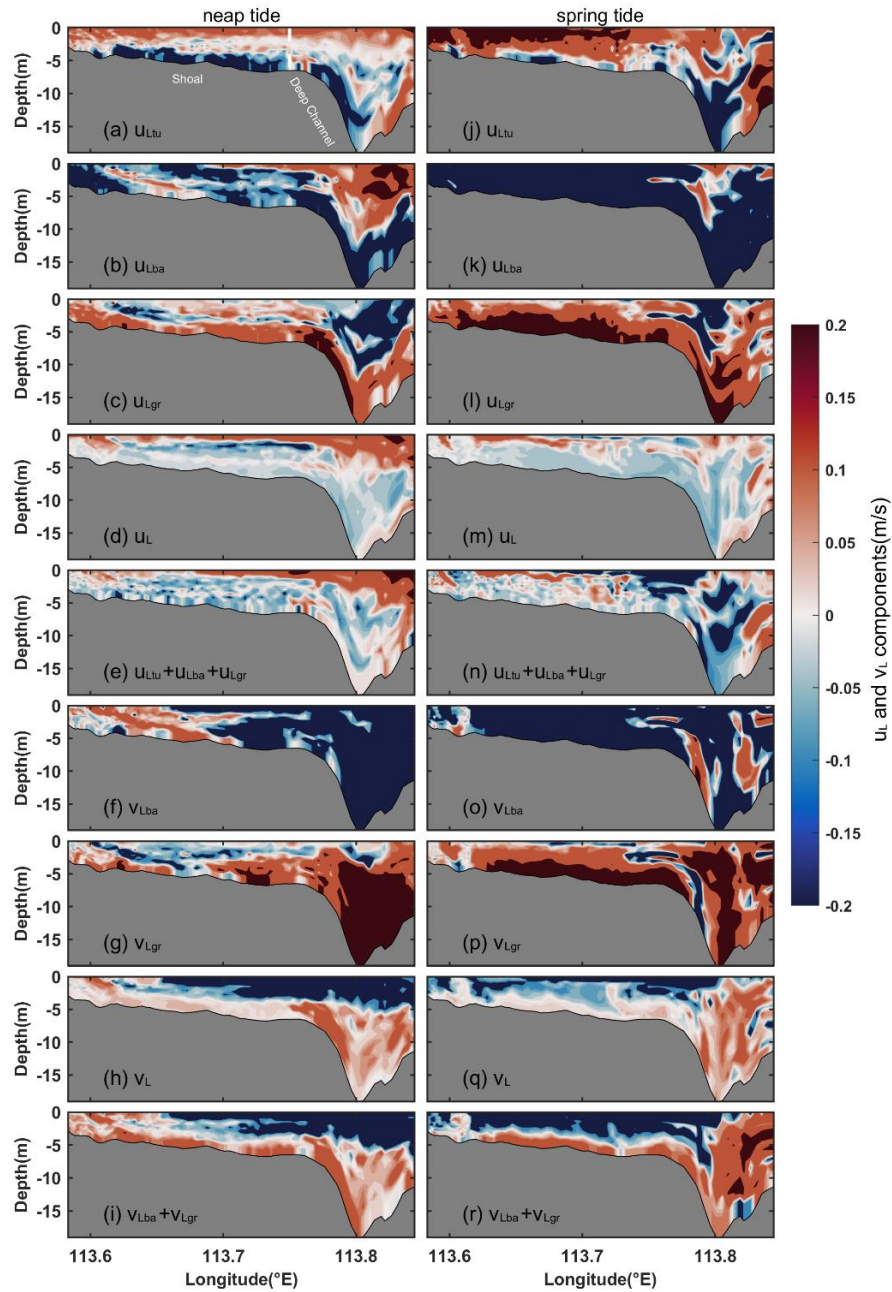
Figure 4 Dominant components of u_L and v_L in Section C for Case 1. For cross-estuary components: **(a, j)** eddy viscosity component (u_{Ltu}), **(b, k)** barotropic component (u_{Lba}), **(c, l)** baroclinic component (u_{Lgr}), **(d, m)** total LRV (u_L) directly obtained by the model, and **(e, n)** cumulative sum of u_{Ltu}, u_{Lba}, and u_{Lgr}. For along-estuary components: **(f, o)** barotropic pressure gradient component (v_{Lba}), **(g, p)** baroclinic pressure gradient component (v_{Lgr}), **(h, q)** total LRV (v_L) obtained directly by the model, and **(i, r)** cumulative sum of v_{Lba} and v_{Lgr}. The components during **(a–i)** represent neap tides, while those during **(j–r)** represent spring tides. For cross-estuary components, red shading indicates eastward flow, and blue shading indicates westward flow. For along-estuary components, red shading signifies inflow, while blue shading denotes outflow.
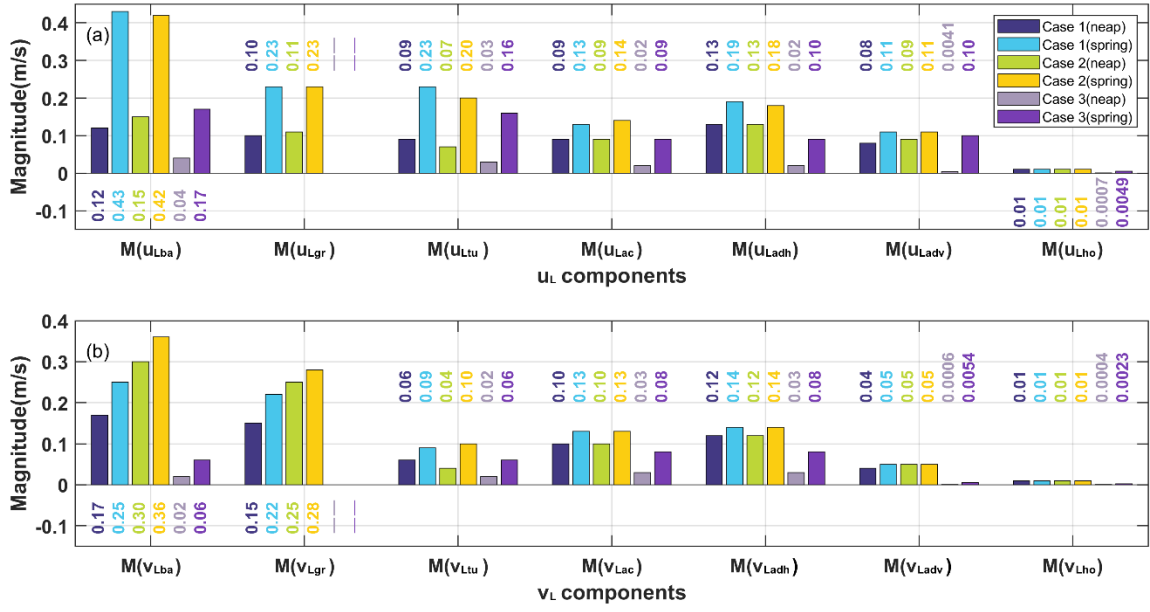
Figure 5 Bar charts for the magnitude of each component of u_L and v_L.
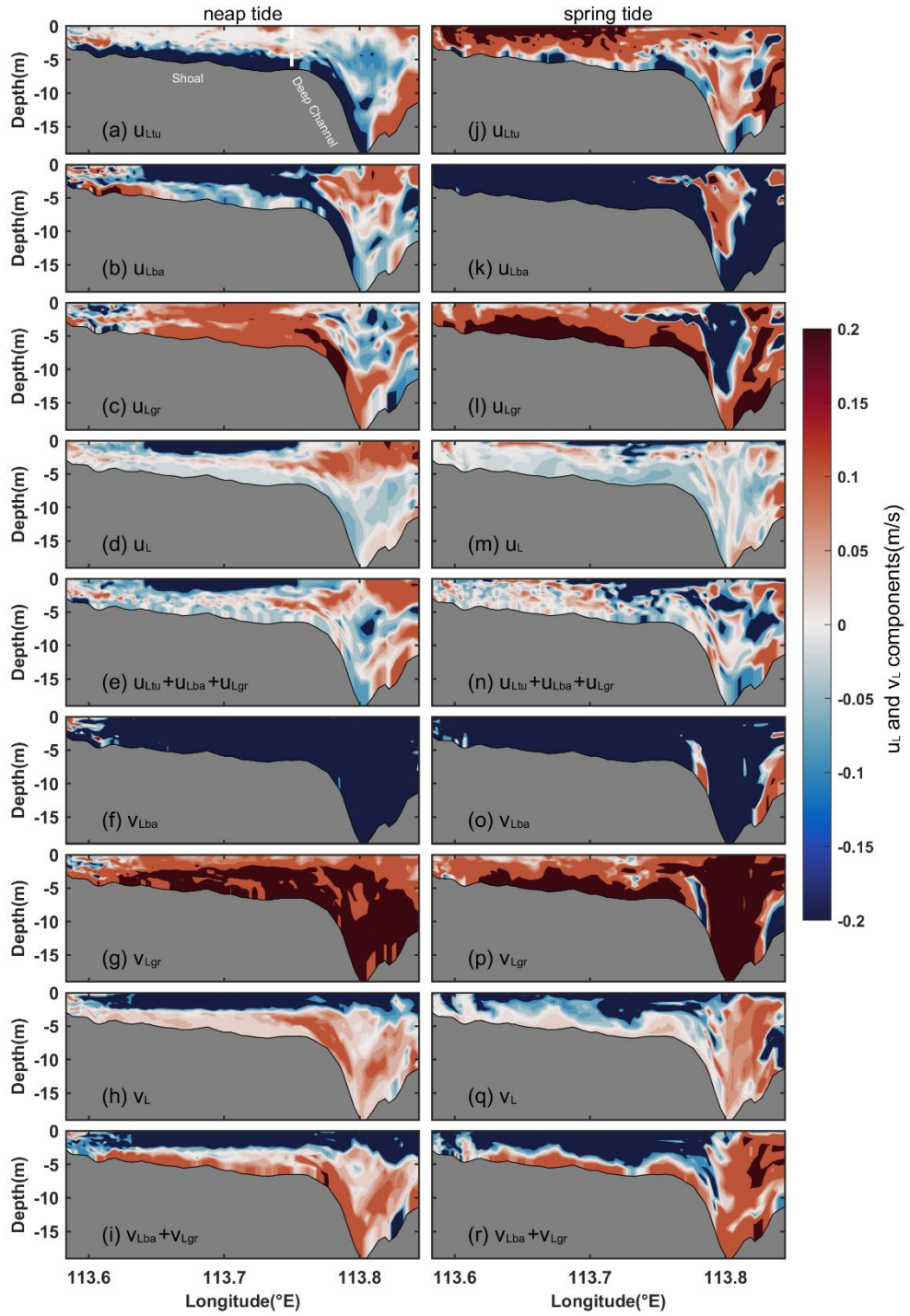
Figure 6 Same as Fig. 4, but for Case 2 without wind forcing.
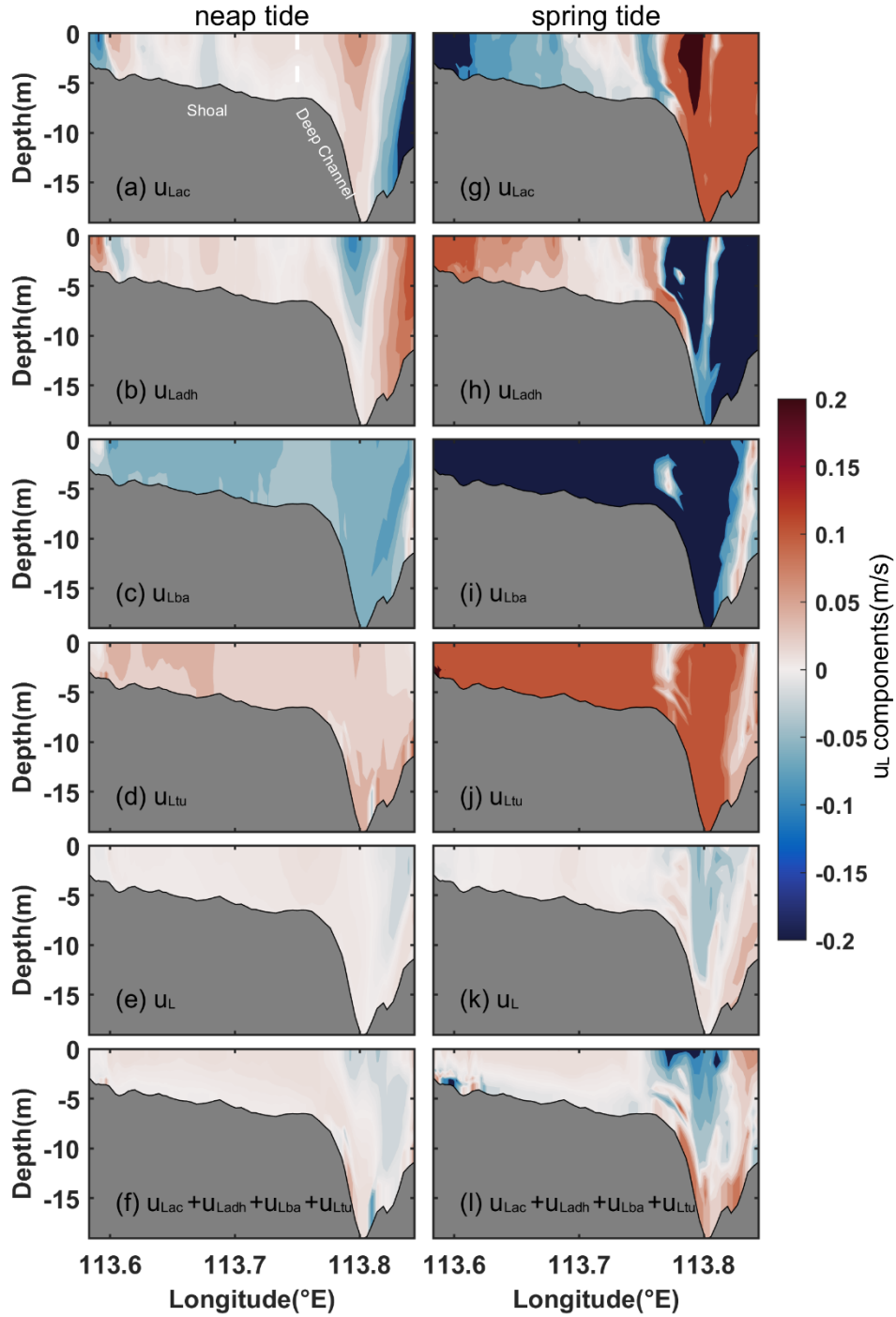
Figure 7 Dominant components of u_L in Section C for Case 3. **(a, g)** Local acceleration component (u_{Lac}), **(b, h)** horizontal nonlinear advection component (u_{Ladh}), **(c, i)** barotropic pressure gradient component (u_{Lba}), **(d, j)** eddy viscosity component (u_{Ltu}), **(e, k)** the total LRV (u_L) obtained directly by the model, and **(f, l)** the sum of u_{Lac}, u_{Ladh}, u_{Lba}, and u_{Ltu} during **(a–f)** neap and **(g–l)** spring tides, respectively. Red shading represents eastward flow and blue shading represents westward flow.
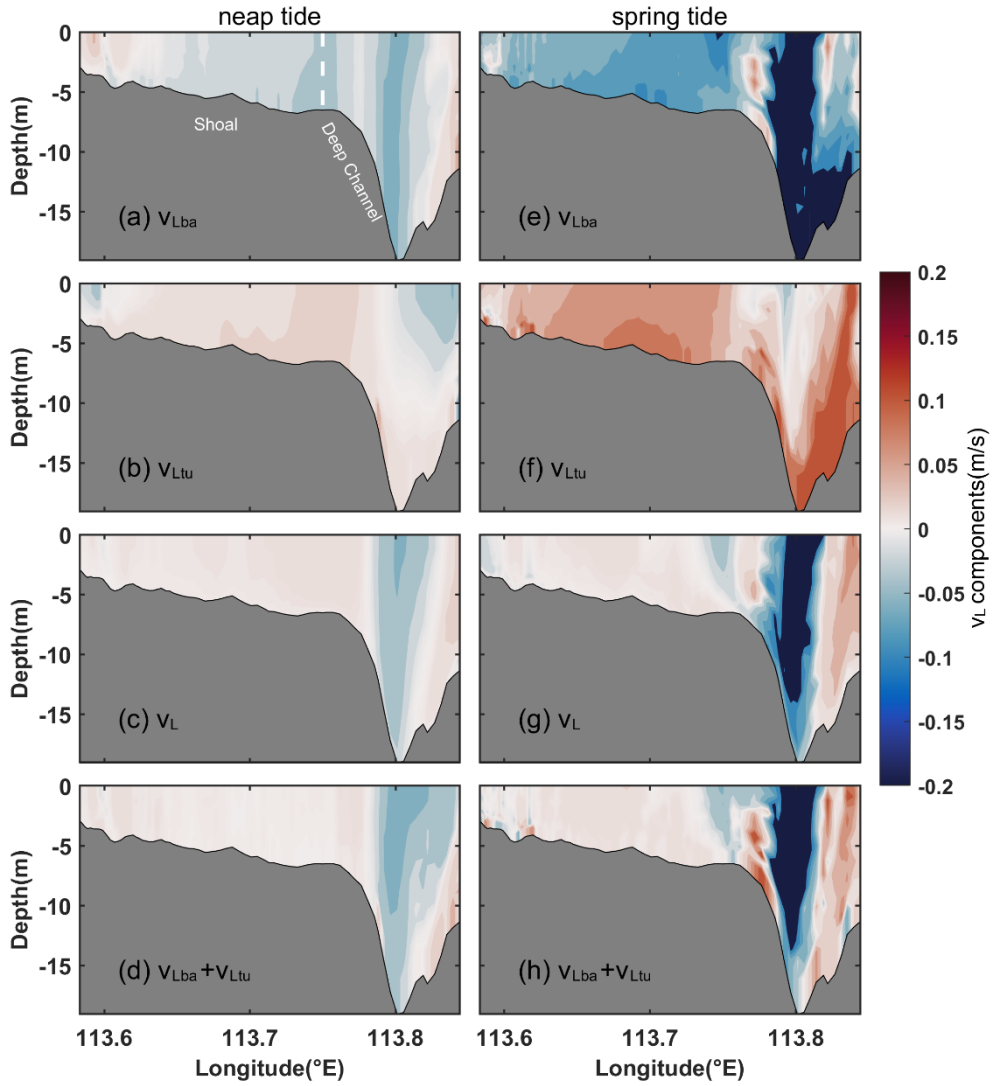
Figure 8 Dominant components of v_L in Section C for Case 3. **(a, e)** Barotropic pressure gradient component (v_{Lba}), **(b, f)** eddy viscosity component (v_{Ltu}), **(c, g)** total LRV obtained directly by the model, and **(d, h)** the sum of v_{Lba} and v_{Ltu} during **(a–d)** neap and **(e–h)** spring tides, respectively. Red shading represents inflow, and blue shading represents outflow.
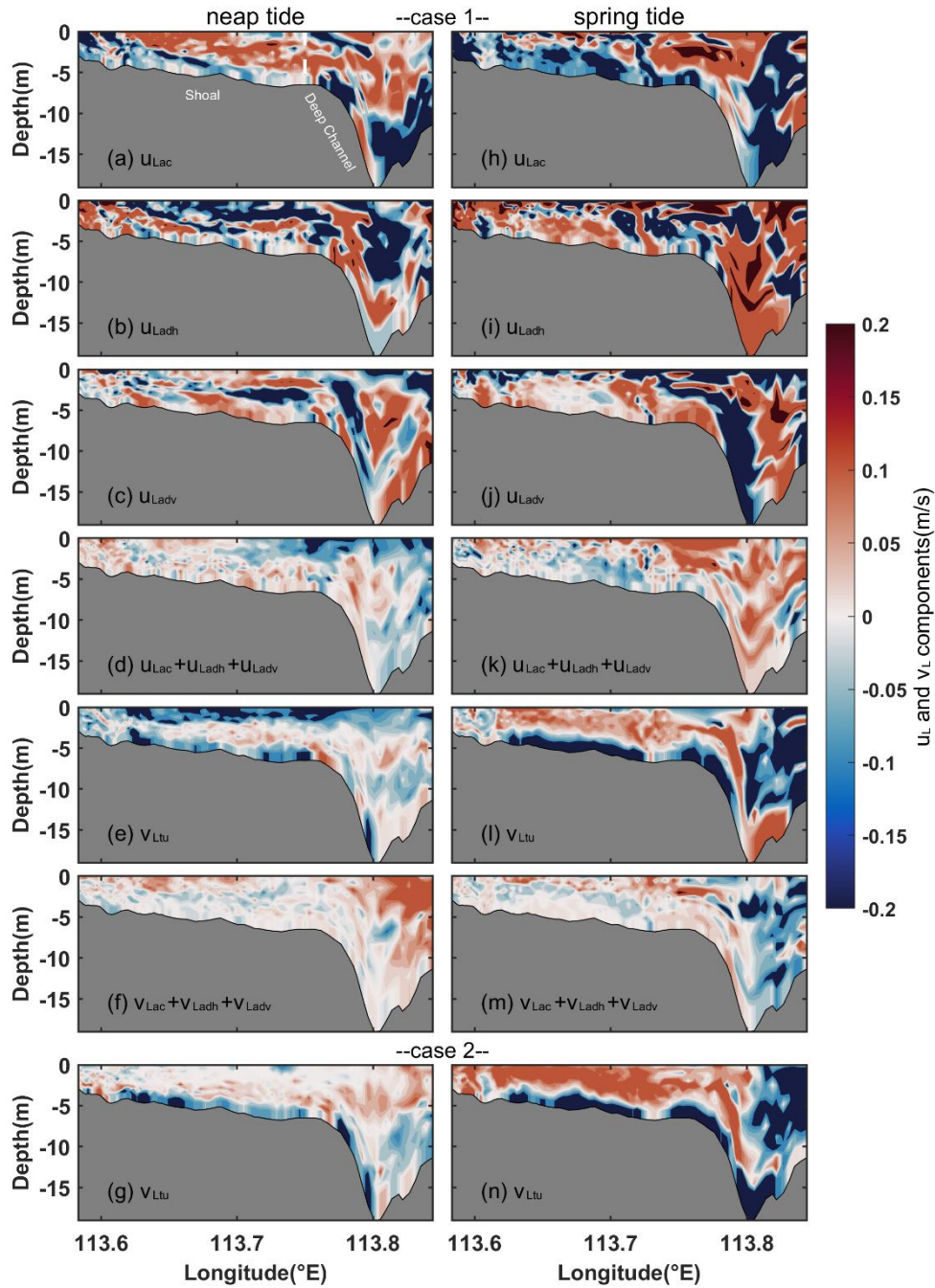
Figure 9 Non-dominant components of u_L and v_L in Section C for Cases 1 and 2. For cross-estuary components in Case 1: **(a, h)** local acceleration component (u_{Lac}), **(b, i)** horizontal nonlinear advection component (u_{Ladh}), **(c, j)** vertical nonlinear advection component (u_{Ladv}), and **(d, k)** the sum of u_{Lac}, u_{Ladh}, and u_{Ladv} during **(a–d)** neap and **(h–k)** spring tides, respectively; for along-estuary components in Case 1: **(e, l)** eddy viscosity component (v_{Ltu}), **(f, m)** the sum of v_{Lac}, v_{Ladh}, and v_{Ladv} during **(e, f)** neap and **(l, m)** spring tides, respectively. Along-estuary **(g, n)** eddy viscosity component (v_{Ltu}) in Case 2 during **(g)** neap and **(n)** spring tides, respectively. The shading follows the same indications as presented in Fig. 1.
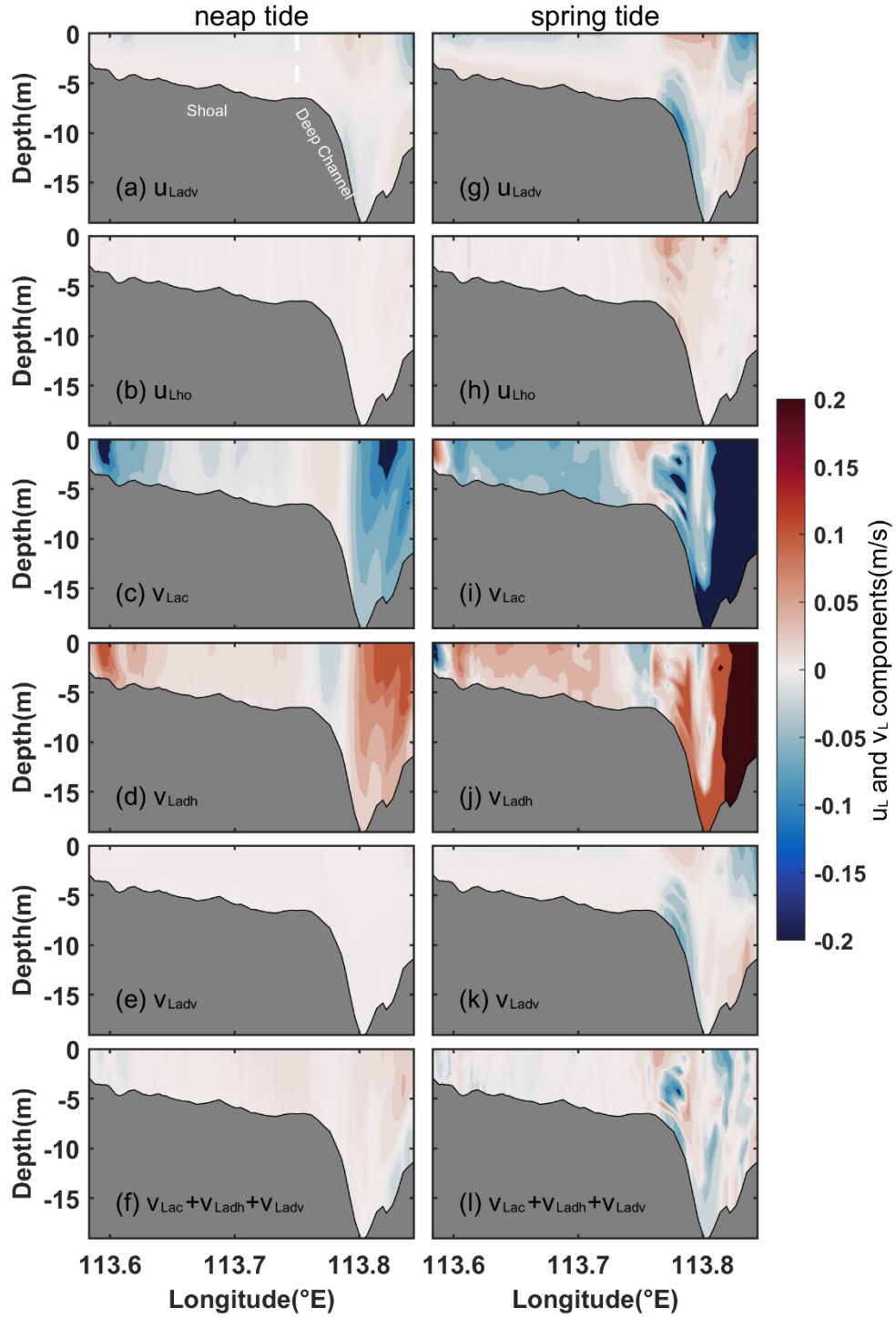
Figure 10 Non-dominant components of u_L and v_L in Section C for Case 3. For cross-estuary components: **(a, g)** vertical nonlinear advection component (u_{Ladv}), **(b, h)** horizontal diffusion component (u_{Lho}); for along-estuary components: **(c, i)** local acceleration component (v_{Lac}), **(d, j)** horizontal advection component (v_{Ladh}), **(e, k)** vertical advection component (v_{Ladv}), and **(f, l)** the sum of v_{Ladc}, v_{Ladh} and v_{Ladv}, during **(a–f)** neap and **(g–l)** spring tides, respectively. The shading follows the same indications as presented in Fig. 1.
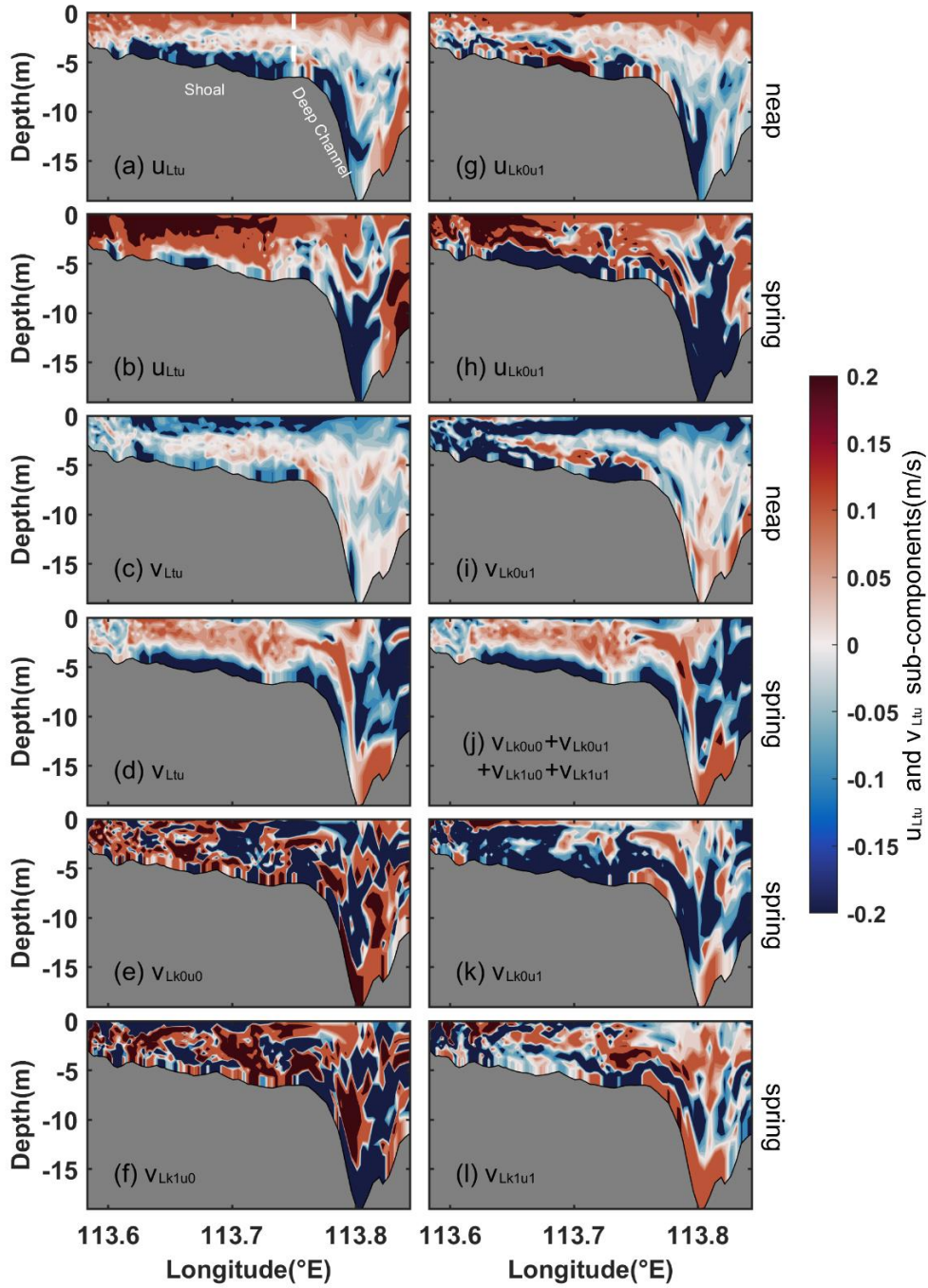
Figure 11 Vertical section of cross-estuary (u_{Ltu}) and along-estuary (v_{Ltu}) eddy viscosity components along with their corresponding dominant subcomponents in Section C for Case 1. The u_{Ltu} during **(a)** neap and **(b)** spring tides, and **(g, h)** the corresponding turbulent mean component (u_{Lk0u1}). **(c)** v_{Ltu} and **(i)** the corresponding turbulent mean component (v_{Lk0u1}) during neap tides, and **(d)** v_{Ltu} and **(j)** the sum of four dominant subcomponents **(e, f, k, and l)** during spring tides. The shading follows the same indications as presented in Fig. 1.
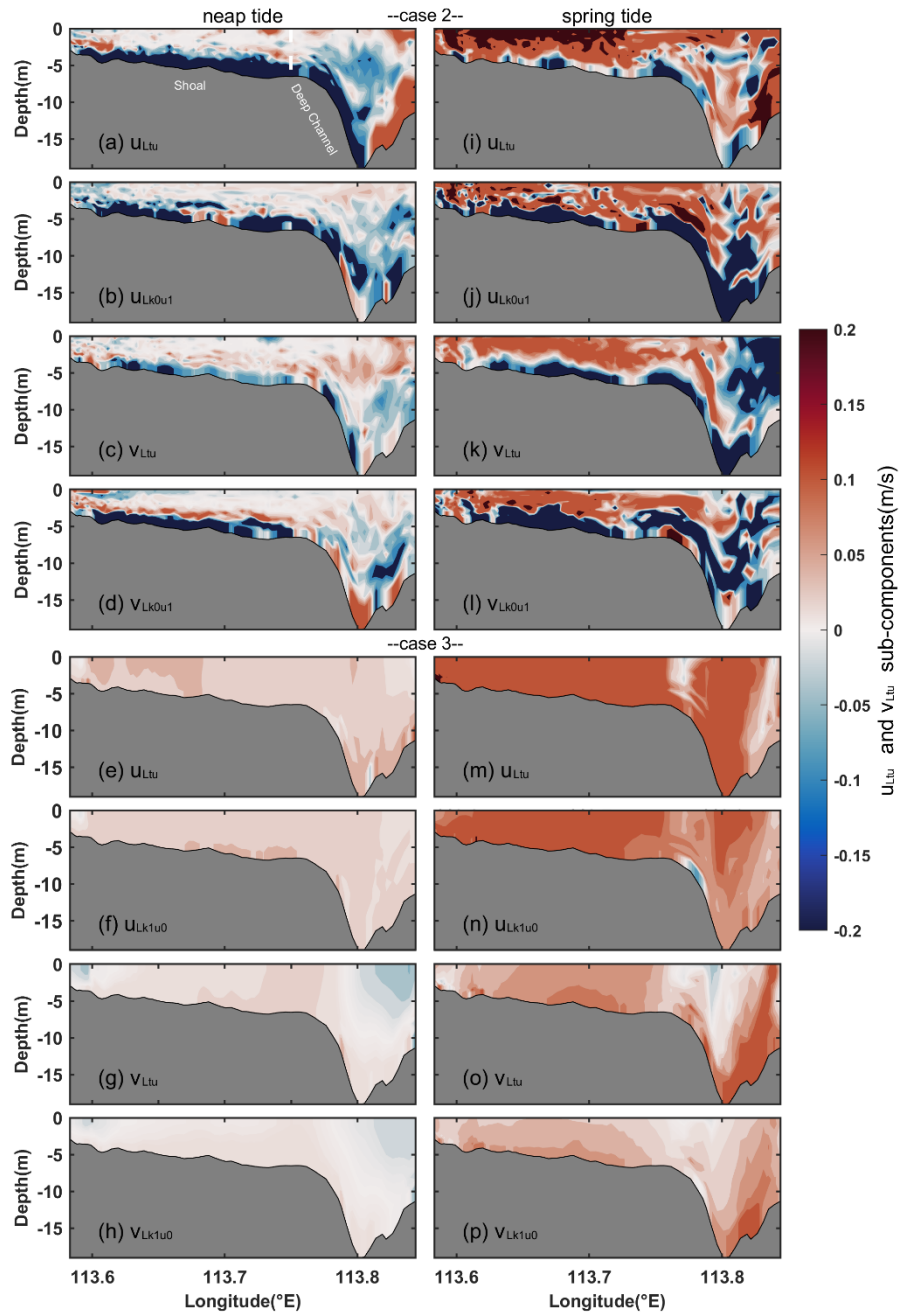
Figure 12 The structure of cross-estuary (u_{Ltu}) and along-estuary (v_{Ltu}) eddy viscosity components and the corresponding dominant components in Section C for Cases 2 **(a–d and i–l)** and 3 **(e–h, and m–p)**. For Case 2: the u_{Ltu} during **(a)** neap and **(i)** spring tides, and **(b, j)** the corresponding turbulent mean component (u_{Lk0u1}); the v_{Ltu} during **(c)** neap and **(k)** spring tides, and **(d, l)** the corresponding turbulent mean component (v_{Lk0u1}). For Case 3: the u_{Ltu} during **(e)** neap and **(m)** spring tides, and **(f, n)** the corresponding tidal straining component (u_{Lk1u0}); the v_{Ltu} during **(g)** neap and **(o)** spring tides, and **(h, p)** the corresponding tidal straining component (v_{Lk1u0}). The shading follows the same indications as presented in Fig. 1.
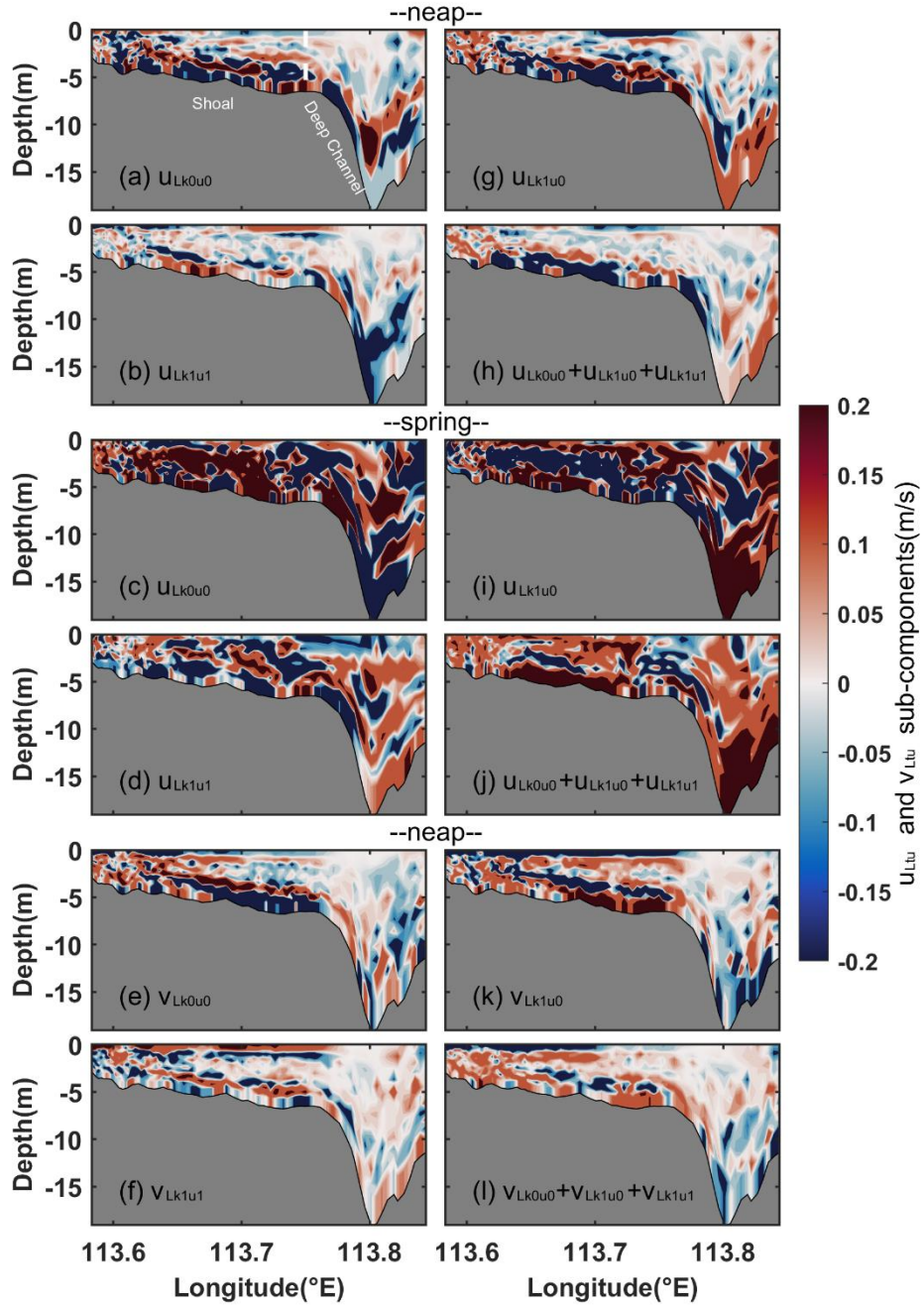
Figure 13 Vertical profiles of non-dominant subcomponents of cross-estuary (u_{Ltu}) and along-estuary (v_{Ltu}) eddy viscosity components for Case 1. For cross-estuary subcomponents: **(a, c)** coupled component of the tidal-average eddy viscosity and velocity gradient oscillation (u_{Lk0u0}), **(g, i)** tidal straining component (u_{Lk1u0}), **(b, d)** coupled component of eddy viscosity oscillation and the tidal-average velocity gradient (u_{Lk1u1}), **(h, j)** the sum of the three subcomponents during neap **(a, b, g, h)** and spring **(c, d, i, j)** tides, respectively. **(e, k, f, l)** Corresponding along-estuary eddy viscosity subcomponents during neap tides.
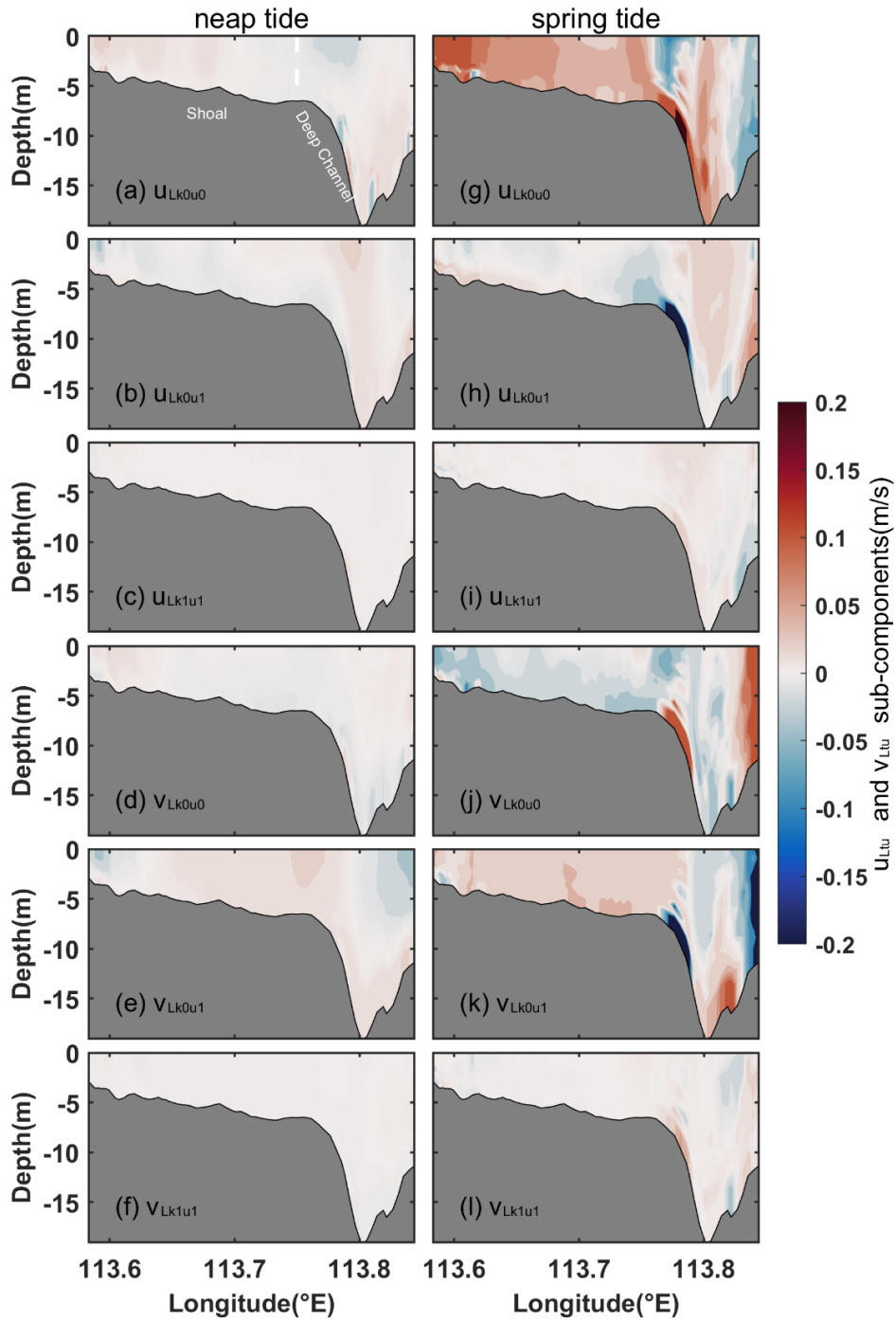
Figure 14 Vertical profiles of non-dominant subcomponents of cross-estuary (u_{Ltu}) and along-estuary (v_{Ltu}) eddy viscosity components for Case 3. For cross-estuary subcomponents: **(a, g)** coupled component of the tidal-average eddy viscosity and velocity gradient oscillation (u_{Lk0u0}), **(b, h)** turbulent mean component (u_{Lk0u1}), **(c, i)** coupled component of eddy viscosity oscillation and the tidal-average velocity gradient (u_{Lk1u1}) during neap **(a–c)** and spring **(g–i)** tides, respectively. **(d, j, e, k, f, l)** Corresponding along-estuary eddy viscosity subcomponents.